



# Synthesis of cobalt ferrite and simultaneous determination of ascorbic acid, acetaminophen and caffeine by voltammetric method using cobalt ferrite modified electrode

Phan Thi Kim Thu<sup>1,2</sup> · Nguyen Duy Trinh<sup>3</sup> · Nguyen Thi Vuong Hoan<sup>4</sup> · Dang Xuan Du<sup>5</sup> · Tran Xuan Mau<sup>1</sup> · Vo Huu Trung<sup>1</sup> · Nguyen Hai Phong<sup>1</sup> · Tran Thanh Tam Toan<sup>1</sup> · Dinh Quang Khieu<sup>1</sup> 

Received: 24 April 2019 / Accepted: 17 August 2019 / Published online: 26 August 2019  
© Springer Science+Business Media, LLC, part of Springer Nature 2019

## Abstract

In the present article, the synthesis of spherical hollow cobalt ferrite and application as an electrode modifier were demonstrated. The synthesis of cobalt ferrite was conducted using carbonaceous microspheres prepared from a glucose solution as a sacrificial template, followed by subsequent heat treatment. The Fe/Co molar ratio in cobalt ferrite depends significantly on the initial Fe/Co molar ratio. The Fe/Co molar ratio as 1/1 could provide the stoichiometric cobalt ferrite ( $\text{CoFe}_2\text{O}_4$ ) with a hollow sphere structure and large saturation magnetization. The simultaneous quantification of ascorbic acid (ASA), acetaminophen (ACE), and caffeine (CAF) was performed utilizing the differential pulse anodic stripping voltammetric method with  $\text{CoFe}_2\text{O}_4$  modified glassy carbon electrode. The detection limits in the linear range of 0.2–4.4  $\mu\text{M}$  are 0.313, 0.267, and 0.226  $\mu\text{M}$  for ASA, ACE, and CAF, respectively. This proposed method enables the simultaneous detection of ASA, ACE, and CAF in pharmaceutical formulations and beverage samples. The determined concentration of the analytes is comparable with that obtained with HPLC.

## 1 Introduction

Ascorbic acid (ASA), also known as vitamin C or L-ascorbic acid (Fig. 1a), is a vitamin found in pharmaceutical formulations and several foods, and it is sold as a dietary supplement. Ascorbic acid is a common enzymatic cofactor in the preparation of collagen, as well as an excellent reductive agent capable of fast quenching several reactive oxygen species [1]. It is a water-soluble vitamin, and its excess in the blood is quickly released in the urine, so it manifests significantly low toxicity. Acetaminophen (ACE), also known

as paracetamol or *N*-acetyl-para-aminophenol (Fig. 1b), is widely used as analgesic and antipyretic drugs. Higher doses may lead to toxicity. Untreated acetaminophen overdose results in a lengthy, painful illness and liver failure. Caffeine (CAF), also known as methyltheobromine or 1,3,7-trimethylxanthine (Fig. 1c) is a central nervous system stimulant of the methylxanthine class [2]. It is the world's most widely consumed psychoactive drug. Caffeine is also a common ingredient in soft drinks, such as cola. Caffeine overdose can result in a state of central nervous system overstimulation, called caffeine intoxication [3]. Ascorbic acid, ACE and CAF exist simultaneously in pharmaceutical formulations or beverages. For example, analgesics such as propyphenazone/paracetamol/caffeine enhances pain reliefs; ASA and CAF can be present in some drinks.

Developing an analytical approach for straightforward, precise and simultaneous quantification of these analytes in food and drug formulations is very challenging. In this view, the voltammetric methods have such an advantage that they can simultaneously analyze these species in the samples. The voltammetric methods with chemically modified electrodes are widely recognized as a robust approach for trace analysis of organic and inorganic species due to high selectivity, sensitivity, and in situ performance. Glassy carbon electrodes

✉ Dinh Quang Khieu  
dqkhieu@hueuni.edu.vn

<sup>1</sup> University of Sciences, Hue University, Hue 530000, Vietnam

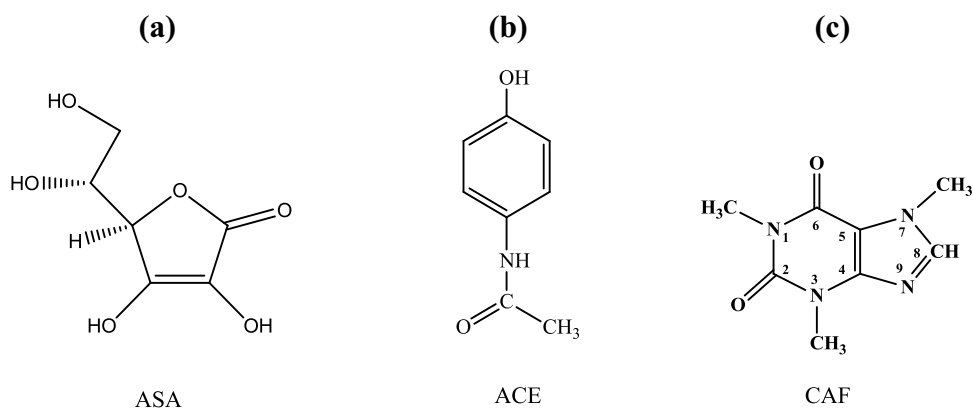
<sup>2</sup> Junior College of Education, Daklak 630000, Vietnam

<sup>3</sup> NTT Hi-Tech Institute, Nguyen Tat Thanh University, Ho Chi Minh City 70000, Vietnam

<sup>4</sup> Faculty of Chemistry, Quy Nhon University, Quy Nhon 590000, Vietnam

<sup>5</sup> Faculty of Natural Sciences, Sai Gon University, Ho Chi Minh City 700000, Vietnam

**Fig. 1** Molecular structure of **a** ASA, **b** ACE, and **c** CAF



(GCEs) are advantageous over other electrodes because the surface modification and renewal can take place simultaneously. The purpose of the electrode surface modification is to increase the electroactive areas and active adsorptive sites and enhance the selective interactions between the modified electrode and the analytes. The electrode modifiers, including carbon nanotubes (CNTs) [4, 5], graphene-based materials [6], orderly mesoporous materials (SBA-15, MCM-41, etc.) [7, 8], nano metal oxides [9, 10], and metal–organic frameworks (MOFs) [11, 12], have widely been used due to their high surface area, high-ordered porous structure, and an abundant number of electrocatalytic sites. Concerning ASA, ACE, and CAF, a few articles have dealt with determining one or two of them together only. A voltammetric determination of ACE using the  $C_{60}$ -modified electrode was carried out by Goyal and Singh [13]; a CNTs modified glassy-carbon electrode was used as an electrochemical sensor for the simultaneous detection of ASA and CAF [4]. Dalmaso et al. [14] reported a simultaneous determination of ASA and ACE in pharmaceutical formulations using a modified GCE with CNTs dispersed in polyhistidine. Because direct redox reactions occur at very similar potentials on bare GCE electrodes, the determination of each species results in a rather poor selectivity. This is a problem because some pharmaceutical formulations or drinks often contain two of these three species [15, 16]. Recently, Fernandes et al. [15] use manganese ferrite/nitrogen-doped CNTs as an electrode modifier for the simultaneous determination of ASA, ACE, and CAF. Khoshhesab [17] fabricates a new CuO-graphene modified electrode for the simultaneous electrochemical determination of ASA, ACE, and CAF.

Cobalt ferrite ( $CoFe_2O_4$ ) with an inverse spinel structure displays ferrimagnetic property that generates from the magnetic moment of anti-parallel spins between  $Co^{2+}$  ions at octahedral sites and  $Fe^{3+}$  ions at tetrahedral sites [6]. Cobalt ferrite has unique physicochemical properties that make it a promising material in antenna rods manufacturing, catalysis, magnetic data storage, sensors, energy conversion applications, and targeted drug delivery [18, 19]. The synthetic ways for

$CoFe_2O_4$  nanoparticles such as sol–gel [20], combustion [21], microemulsion [22], thermal decomposition [23], micelles and reverse micelles co-precipitation [24], mechanical alloying [25], hydrothermal [26], and electrochemical procedures [21, 27] have been intensively investigated. These synthetic ways aim to reduce the calcination temperature, to form a hierarchical structure, and to prevent agglomeration. Cobalt ferrite thus synthesized has high specific magnetization, high crystallinity, small agglomeration, and large surface area. Recently, the synthesis of hollow-sphere oxides using sacrificial templates has been developed significantly. Colloidal nanoparticles (e.g., Au, Ag, or CdS) have been used as templates, in which the desired metal ions are introduced into composite core–shell structures, and these are then transferred into hollow capsules utilizing chemical or thermal treatment [28–30]. Sun et al. [31] report employing carbonaceous polysaccharide microspheres as templates for the preparation of metal-oxide hollow spheres ( $CoO$ ,  $Al_2O_3$ ,  $Ga_2O_3$ ,  $NiO$ ,  $Mn_3O_4$ ,  $Cr_2O_3$ ,  $La_2O_3$ ,  $Y_2O_3$ ,  $Lu_2O_3$ ,  $TiO_2$ , and  $ZrO_2$ ). To our best knowledge, only a few articles have been published concerning new cobalt ferrite-modified electrodes for the simultaneous determination of ASA, ACE, and CAF.

In our previous article, we demonstrate the simultaneous determination of ASA, ACE, and CAF on electrochemically reduced graphene oxide modified electrodes [32]. To further develop the point, the in situ synthesis of cobalt ferrite with hollow-sphere structure was performed using a sacrificial spherical carbon template. The resulting cobalt ferrite was used as an electrode modifier to simultaneously determine ASA, ACE, and CAF. The electrode reaction kinetics and application to real samples were also addressed.

## 2 Experimental

### 2.1 Materials

D-glucose ( $C_6H_{12}O_6$ , 99.5%), cobalt nitrate hexahydrate ( $Co(NO_3)_2 \cdot 6H_2O$ , 98%), ferrous sulfate heptahydrate

( $\text{FeSO}_4 \cdot 7\text{H}_2\text{O}$ , 99%), and ethanol ( $\text{C}_2\text{H}_5\text{OH}$ , 99%) were purchased from the Merck Company, Germany and used to synthesize cobalt ferrite. Potassium hydroxide (KOH), phosphoric acid ( $\text{H}_3\text{PO}_4$ , 85%), potassium dihydrogen phosphate ( $\text{KH}_2\text{PO}_4$ , 99%), and boric acid ( $\text{H}_3\text{BO}_3$ , 99%) were obtained from Daejung, Korea and used to prepare the buffer solution. The Britton–Robinson buffer solutions (B–R BS) were prepared from 0.5 M  $\text{H}_3\text{BO}_3$ , 0.5 M  $\text{H}_3\text{PO}_4$ , and 0.5 M  $\text{CH}_3\text{COOH}$  solutions. The desired pH of the B–R buffer was adjusted using 1 M KOH or 1 M  $\text{H}_3\text{PO}_4$  solutions. Paracetamol ( $\text{C}_8\text{H}_9\text{NO}_2$ , 99%), caffeine ( $\text{C}_{18}\text{H}_{10}\text{N}_4\text{O}_2$ , 98.5%), and ascorbic acid ( $\text{C}_8\text{H}_6\text{O}_6$ , 99.7%) were purchased from Merck Company, Germany. The stock solutions (10 mM) of ASA, ACE, and CAF were prepared just prior to use to avoid any decomposition.

## 2.2 Cobalt ferrite preparation

Cobalt ferrite was synthesized according to Wang et al. [28, 33]. Glucose (4 g, 0.022 mol) was dissolved in distilled water (40 mL) to form a homogeneous solution. Then, the mixture of 0.02 mol of the two salts (Fe:Co = 0.5:1; 0.95:1; 0.96:1; 0.97:1; 1:1; 2:1 (mol/mol)) was added to the glucose solution. The resulting solution was sealed in a 40 mL autoclave with a Teflon seal and maintained at 180 °C for 8 h to form black solids. The solids were then separated using centrifugation at 5000 rpm. A refining process using five cycles of centrifugation/washing/redispersion was performed with water or ethanol. The as-synthesized cobalt ferrite/carbon was dried at 100 °C and, then calcinated at 500 °C for 5 h to obtain cobalt ferrite with different Fe/Co molar ratios (see Fig. 2). Carbonaceous microspheres were also synthesized with this procedure without the addition of the metal salts.

## 2.3 Apparatus

X-ray diffraction (XRD) analysis was performed on a D8 Advanced Bruker anode X-ray Diffractometer with  $\text{CuK}\alpha$

( $\lambda = 1.5406 \text{ \AA}$ ) radiation. Photoelectron spectrometry (XPS) was conducted on ESCA La 250. Nitrogen adsorption/desorption isotherms were measured using a Micromeritics 2020 volumetric adsorption analyzer system. The samples were degassed by heating under vacuum at 150 °C for 3 h. The specific surface area of the samples was calculated using the Brunauer–Emmett–Teller (BET) model. Diffusive reflectance UV–Vis spectroscopy (DR–UV–Vis) was conducted on JASCO-V670 at 200–800 nm. X-ray photoelectron spectroscopy (XPS) was conducted on a Shimadzu Kratos AXISULTRA DLD spectrometer equipped with the Theta Probe AR–XPS System (Thermo Fisher Scientific, U.K). The magnetic property was analyzed using a vibrating sample magnetometry (VSM, Micro Sence Easy VSM 20130321-02) at ambient temperature.

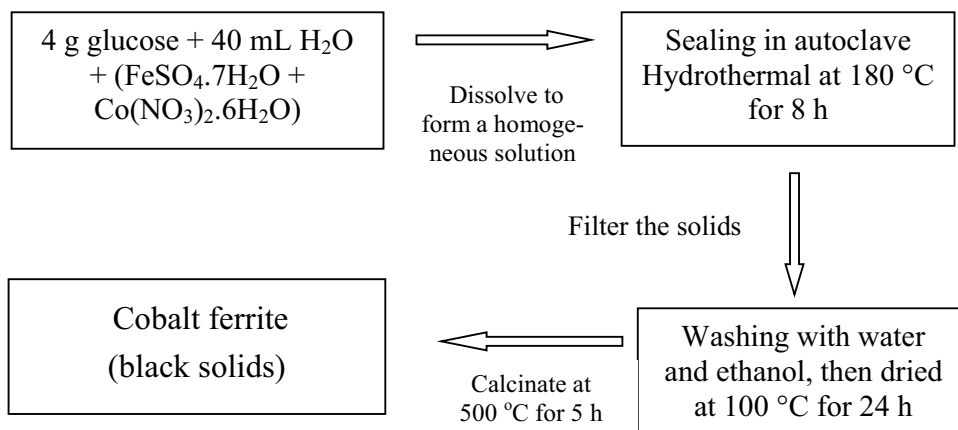
The determinations of ASA, ACE, and CAF were performed using a Shimadzu 2030 HPLC system with a UV–Vis detector ( $\lambda = 275 \text{ nm}$ ). A C18 (250 × 4 mm; 5  $\mu\text{m}$ ) chromatographic column was employed. The mobile phase is the mixture of a phosphate buffer pH 2.3/acetonitrile (35/65 v/v) at a flow rate of 1.5  $\text{mL min}^{-1}$ , while the injection volume is 5  $\mu\text{L}$ .

The electrochemical experiments include cyclic voltammetry (CV) and differential pulse voltammetry (DPV). They were carried out at ambient temperature using a CPA–HH5 Computerized Polarography Analyzer (Vietnam). A conventional three-electrode cell was employed. The working electrode is a modified and unmodified glassy carbon electrode (GCE) with a diameter of 2.8 mm. The auxiliary and reference electrodes are platinum wire and Ag/AgCl (sat. KCl), respectively.

## 2.4 Preparation and modification of electrode

The working electrode surface was washed with ethanol and polished with alumina slurry (0.05  $\mu\text{m}$ ). The dispersion was then utilized to prepare the modified electrode. Briefly, 0.01 g  $\text{CoFe}_2\text{O}_4$  in 10 mL ethanol was sonicated for

**Fig. 2** Diagram of cobalt ferrite synthesis



48 h. 5  $\mu\text{L}$  of  $\text{CoFe}_2\text{O}_4$  suspension ( $1 \text{ g L}^{-1}$ ) was dropped on the electrode surface and dried in air for 4 h at ambient temperature.

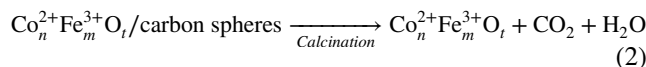
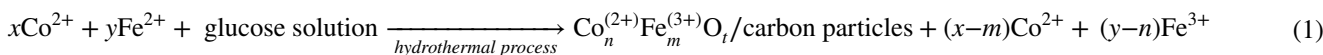
## 2.5 Pharmaceutical preparation

The samples were purchased at a local pharmacy. Six tablets of Acetab Extra, Flucoldstad, Pancelxim Extra, Hapacol Sac. 150 mg Kids, Doliprane, vitamin C 500MG/150MG, Efferalgan, and Vitamin C, and three drinks, namely Number One, Sting max gold, and Wake-up 247, were used in this study. Ten tablets of each of the six pharmaceutical preparations were finely ground in a mortar. An exact amount of the powder was weighed and transferred to a 100 mL calibrated flask, which was filled to the volume with double distilled water. The standard addition method was used for determining the pharmaceutical formulations using the modified electrode. For the beverages, the liquid samples were analyzed directly without any further treatment. 100  $\mu\text{L}$  of the soft drink samples was added to a container containing 0.2 M B–R BS (pH 4) then quantified using the DPV method.

## 3 Results and discussion

### 3.1 Material characterization

In one of our previous studies, we found that the mixture of  $\text{Fe}^{2+}$ ,  $\text{Co}^{2+}$ , and D-glucose could provide cobalt ferrite/carbon hollow spheres while that of  $\text{Fe}^{3+}$ ,  $\text{Co}^{2+}$ , and D-glucose provided two separate phases of the oxides mixture and carbon spheres (SEM not shown here). Hence, the iron(II) source was used in this study. The general reactions are as follows:



The elemental composition of bimetallic oxides ( $\text{Co}_n^{2+}\text{Fe}_m^{3+}\text{O}_t$ ) depends significantly on the initial  $\text{Fe}^{2+}/\text{Co}^{2+}$  molar ratio. A series of experiments with different Fe/Co molar ratios in the initial mixture was performed to synthesize the bimetallic oxides and the Fe/Co molar ratio was determined using EDX. Figure 3a illustrates the EDX analysis of cobalt ferrite with the initial Fe/Co molar ratio of 1/1. Cobalt and iron are observed and a small amount of sulfur is also detected due to impurities. The plot of the Fe/Co molar ratio in the product versus the initial Fe/Co molar ratio is illustrated in Fig. 3b. When the initial Fe/Co molar ratio is low (0.5) or high (2.0), the Fe/Co molar ratio in the calcined product deviates significantly from the stoichiometry of cobalt ferrite ( $\text{CoFe}_2\text{O}_4$ ). When the Fe/Co molar ratio in the synthetic mixture is found approximately 1 (0.95 to 1.01), the Fe/Co molar ratio in the product is approximately 2, and the cobalt ferrite has the formula  $\text{CoFe}_2\text{O}_4$ . Therefore, the initial Fe/Co molar ratio 1/1 was chosen for further experiments.

The resulting specimens were subjected to XRD measurements (Fig. 4). No characteristic diffractions are observed in the spherical carbon samples (Fig. 4a) while the amount of carbon in the carbon spheres estimated by elemental analysis is 65% compared with 40% C in glucose ( $\text{C}_6\text{H}_{12}\text{O}_6$ ). These results indicate that glucose, after the hydrothermal treatment at 180  $^\circ\text{C}$ , forms mainly amorphous carbon. The diffractions of the cobalt ferrite precursor (Fig. 4b) are indexed as a spinel-type according to JCPDS No. 00-002-1045. However, the XRD pattern does not show sufficient diffractions, and a large background indicates that the specimens contain a large amount of amorphous phase. It is worth noting

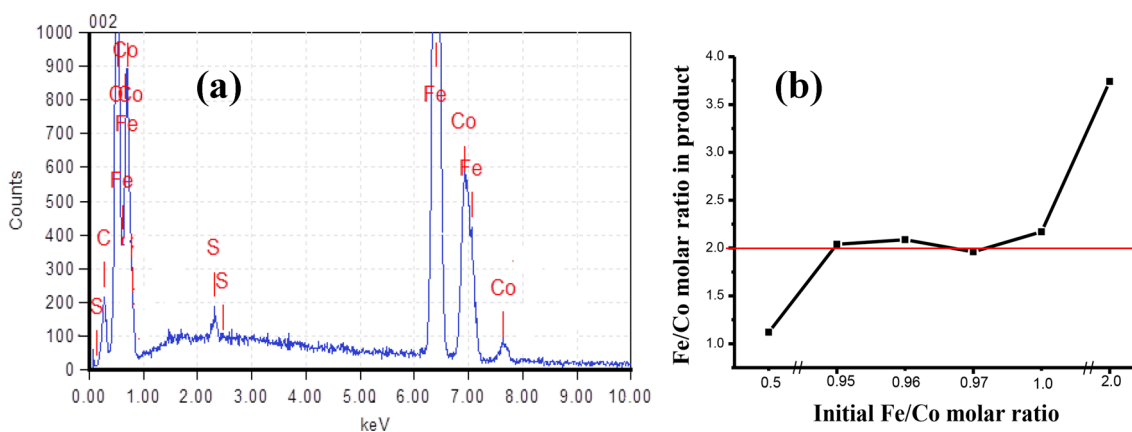


**Fig. 3** **a** EDX of the binary iron-cobalt oxides; **b** effect of the Fe/Co molar ratio in the synthesized gel on the Fe/Co molar ratio of in the calcined products

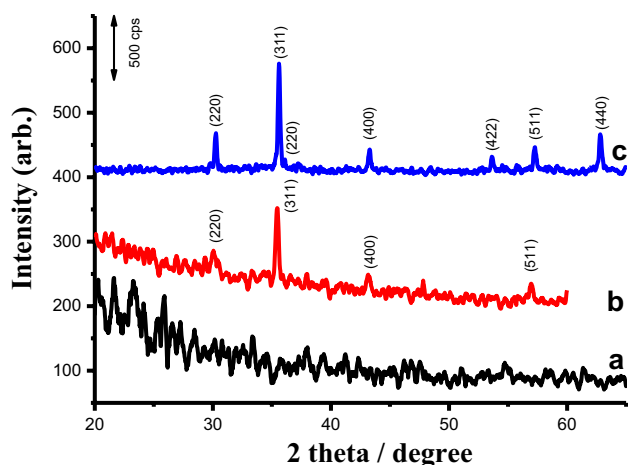


**Fig. 4** XRD patterns of (a) spherical carbon particles; (b) cobalt ferrite precursor; (c) cobalt ferrite (initial Fe/Co molar ratio: 1/1)

that the formation of cobalt ferrite phase normally occurs at high temperatures (700–900 °C) depending on the synthetic approach [34, 35]. Indeed, in the present study, the formation of cobalt ferrite takes place at a low temperature (180 °C) due to the high dispersion of cobalt and iron ions in the glucose medium. The cobalt ferrite precursor calcined

at 500 °C provides fully crystallized cobalt ferrite (Fig. 4c). All the peaks can be assigned to the cobalt ferrite structure. No intermediate phase is observed, inferring that a single-phase cobalt ferrite structure is formed within the sensitivity of experimental measurements. The average crystallite size of  $\text{CoFe}_2\text{O}_4$  particles was calculated using the Scherrer equation  $D_{hkl} = K \cdot \lambda / \cos\theta$ , where  $D_{hkl}$  is the crystallite size estimated from the (311) diffraction peak;  $K$  is the sphere shape factor (0.9);  $\theta$  is the Bragg angle;  $\beta$  is the full-width at half-maximum of the (311) diffraction peak; and  $\lambda$  is the wavelength of the X-ray (1.541 Å). The average crystallite size of  $\text{CoFe}_2\text{O}_4$  ferrite particles in our study is about 33 nm.

Figure 5a shows the SEM image of the carbon particles synthesized with the hydrothermal treatment of glucose at 180 °C. As seen from the figure, the morphology of carbon consists of spherical particles with approximately 5  $\mu\text{m}$  in diameter. The synthetic temperature is higher than the normal glycosidation temperature, which leads to aromatization and carbonization [33, 36, 37]. The SEM image of cobalt ferrite precursor is shown in Fig. 5b. The particles are also spherical with flocculent substances on the surface. This is probably the result of a second nucleus-forming phase taking place on the surface of the carbon spheres. That is, iron/cobalt species form the nuclei on the surface of the carbon spheres in the reaction between cobalt and iron species to

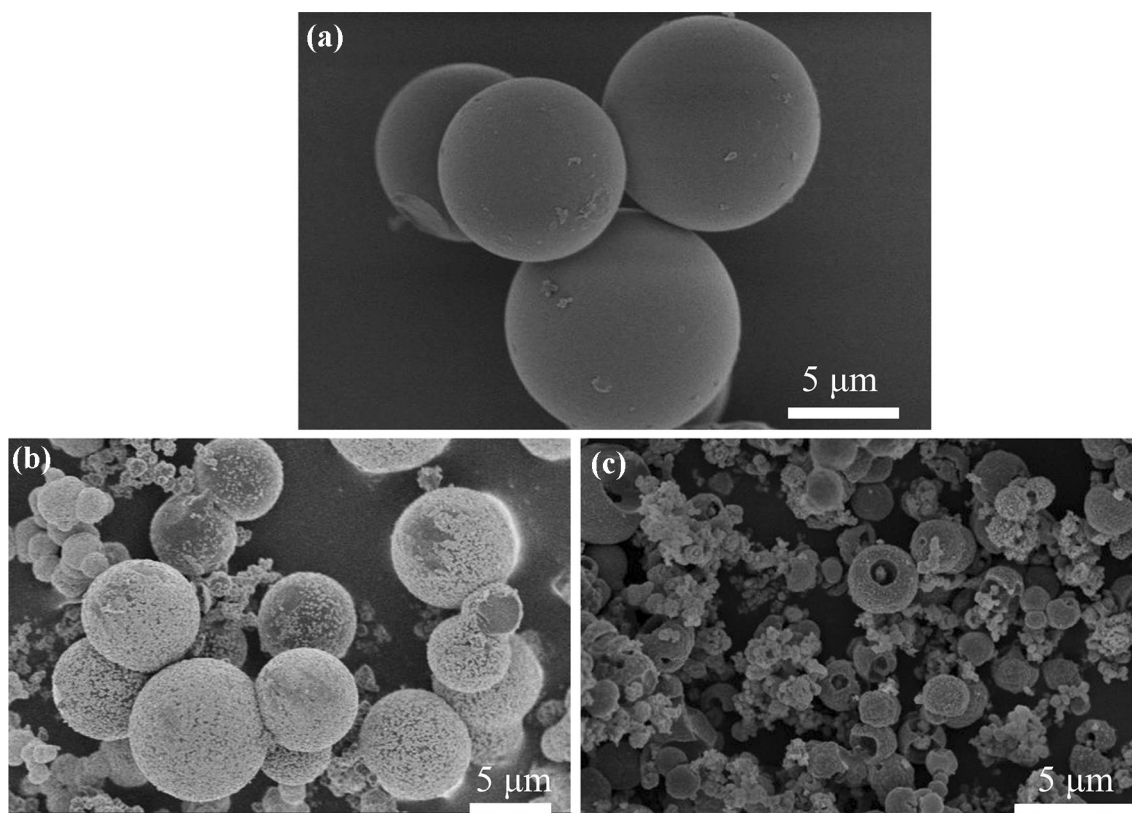


**Fig. 5** SEM observation of **a** spherical carbon particles; **b** cobalt ferrite precursor; **c** cobalt ferrite (initial Fe/Co molar ratio: 2/1)

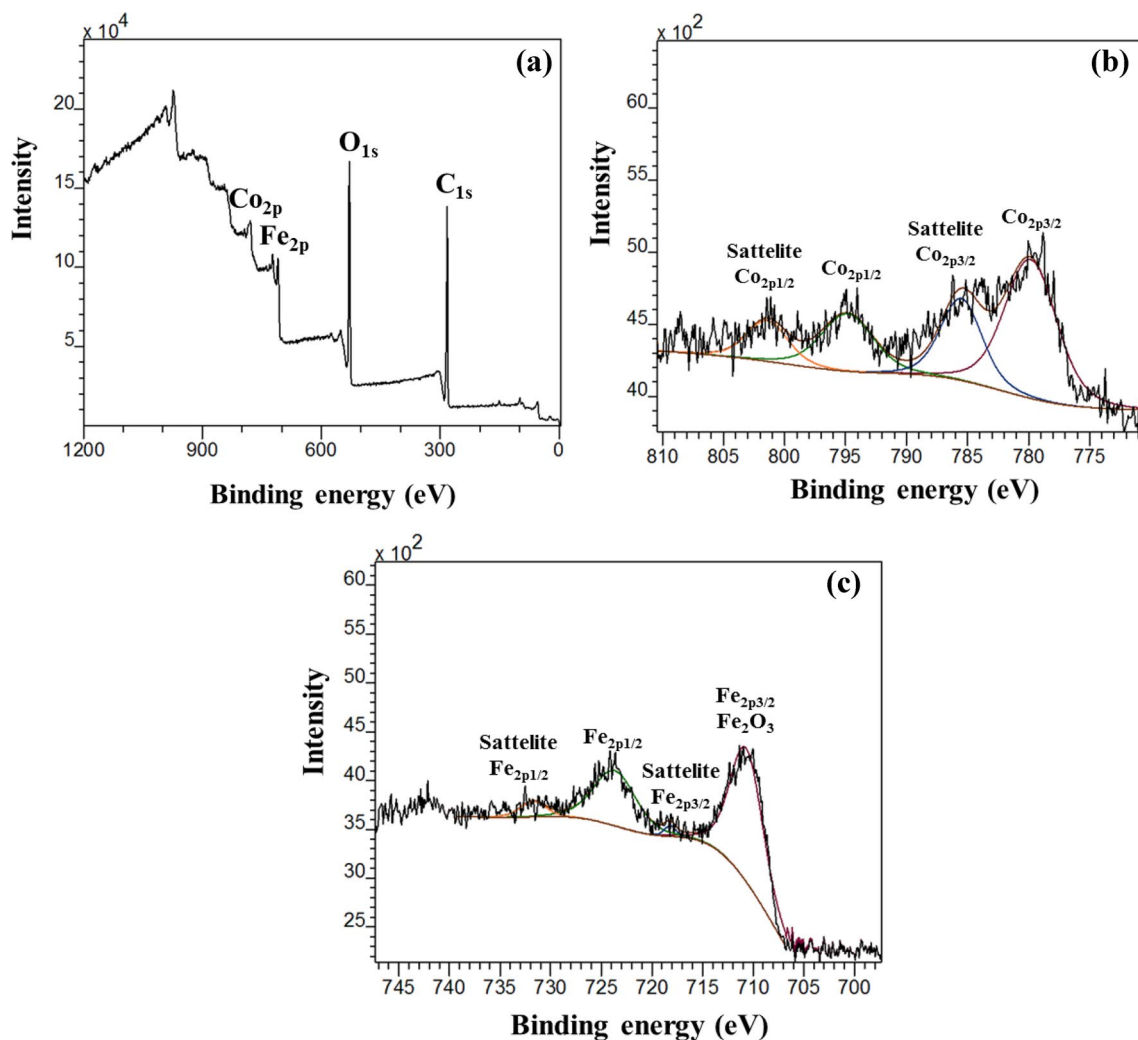
create cobalt ferrite. The carbon spheres act as a sacrificial template and are removed completely from the cobalt ferrite precursor by calcination at 500 °C for 5 h to form cobalt ferrite with a hierarchical structure (hollow spheres) (Fig. 5c).

The XPS spectra of  $\text{CoFe}_2\text{O}_4$  in Fig. 6 show Fe, Co, O, and even C peaks (Fig. 6a). The O 1s signal is detected at 529.94 eV, indicating O bonding with metal and at 531.33 eV for the O–C bond (organic compound) due to the incomplete burning of glucose. The  $\text{Co}2p_{3/2}$  signal appears at 779.85 eV with a satellite peak at 785.51 eV, and  $\text{Co}2p_{1/2}$  signal can be seen at 794.85 eV with a satellite peak at 801.41 eV (Fig. 6b). The peak separation between  $\text{Co}2p_{3/2}$  and  $\text{Co}2p_{1/2}$  is around 15 eV. The separation between the main peak and the satellite peak is  $\sim 5.7$  eV for  $\text{Co}2p_{3/2}$  and  $\sim 6$  eV for  $\text{Co}2p_{1/2}$ . This difference is an important indicator of the oxidation state of the cobalt ion. A narrow separation of about 4–6 eV (found in our study) is a typical characteristic of Co(II), while a larger difference of about

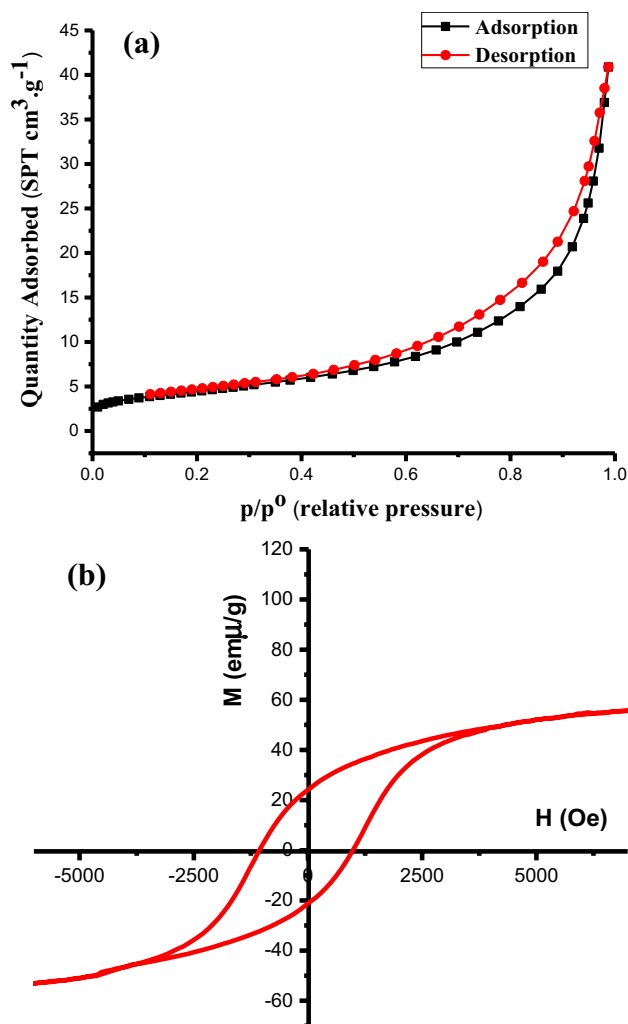
9–10 eV is often found with Co(III) [38]. Therefore, the Co ions in cobalt ferrite are divalent. Fe2p has two signals:  $\text{Fe}2p_{3/2}$  and  $\text{Fe}2p_{1/2}$  that locate at approximately 710.67 eV and 723.67 eV, respectively (Fig. 6c). The presence of the satellite peak at 718.20 and 731.76 eV of  $\text{Fe}2p_{3/2}$  implies the trivalent iron [39]. The XPS analysis again confirms the formula  $\text{CoFe}_2\text{O}_4$  for cobalt ferrite.

Figure 7a presents the nitrogen adsorption/desorption isotherms of cobalt ferrite calcined at 500 °C. The curves show the IV isotherms with an H3 hysteresis loop at the relative pressure ranging from 0.5 to 0.9, which reveals the presence of mesopores and micropores [40, 41]. The specific surface area calculated using the BET model is  $19.46 \text{ m}^2 \text{ g}^{-1}$ .

The magnetic properties of spinel were determined via VSM measurements at ambient temperature (Fig. 7b). The magnetization hysteresis loop exhibits the S-like type. The saturation magnetization value of spinel is  $59 \text{ emu g}^{-1}$ . This value is lower than that of pure nanomagnetic  $\text{Fe}_3\text{O}_4$  [42, 43]



**Fig. 6** The XPS spectra of  $\text{CoFe}_2\text{O}_4$ : **a** survey XPS spectrum; **b**  $\text{Co}2p$ ; **c**  $\text{Fe}2p$



**Fig. 7** **a** Nitrogen adsorption/desorption isotherms; **b** magnetic properties of  $\text{CoFe}_2\text{O}_4$

but compatible with that of the magnetic materials reported in references [44, 45]. The magnetic coercivity is nearly 1000 Oe manifesting that magnetization remains upon the removal of the external magnetic field. Therefore, cobalt ferrite is considered as a ferromagnetic material. It belongs to the hard type due to its large magnetic coercivity, which is useful in permanent magnets.

### 3.2 Electrochemical behavior of $\text{CoFe}_2\text{O}_4$ modified electrode

The Randles–Sevcik equation is widely employed to calculate the active surface area of the electrodes. It is expressed as follows:

$$I_p = (2.69 \times 10^5) \cdot n^{3/2} \cdot A \cdot C \cdot D^{1/2} \cdot \nu^{1/2} \quad (3)$$

where  $I_p$  represents the anodic peak current ( $\mu\text{A}$ );  $n$  is the total number of electrons transferred ( $n=1$ );  $A$  refers to the electroactive surface area of the electrode;  $D$  is the diffusion coefficient of  $1 \text{ mM } \text{K}_3[\text{Fe}(\text{CN})_6]/\text{K}_4[\text{Fe}(\text{CN})_6]$  in  $0.1 \text{ M } \text{KCl}$  ( $7.6 \times 10^{-6} \text{ cm}^2 \text{ s}^{-1}$ );  $C$  is the concentration of  $\text{K}_3[\text{Fe}(\text{CN})_6]/\text{K}_4[\text{Fe}(\text{CN})_6]$  ( $1 \text{ mM}$ ); and  $\nu$  is the scan rate ( $\text{V s}^{-1}$ ).

The electroactive surface area is obtained from the slope of the linear line of  $I_p$  versus  $\nu^{1/2}$  (Fig. 8a–d) and the calculated value for GCE and  $\text{CoFe}_2\text{O}_4/\text{GCE}$  is  $0.043$  and  $0.128 \text{ cm}^2$ , respectively. The increase (almost three times) in the electroactive surface area of the modified electrode is due to the capacity of cobalt ferrite to modify the electrode and implement a large surface and porous structure and thus facilitate the electron transfer between the electrode and the solution.

In the present study, the electrochemical behavior of ASA, ACE, and CAF at bare GCE and  $\text{CoFe}_2\text{O}_4/\text{GCE}$  were studied using CV and DPV. The voltammogram at bare GCE presents broad peaks in redox processes, while at  $\text{CoFe}_2\text{O}_4/\text{GCE}$ , well-defined oxidation peaks of ASA, ACE, and CAF appear at  $0.38$ ,  $0.69$ , and  $1.47 \text{ V}$ , respectively (Fig. 9a). Similar to CV, the DPV curve at bare GCE exhibits broad peaks of anodic stripping voltammetry, while the curve at  $\text{CoFe}_2\text{O}_4/\text{GCE}$  presents well-defined peaks (Fig. 9b). The oxidation peak current for ASA, ACE, and CAF at  $\text{CoFe}_2\text{O}_4/\text{GCE}$  is nearly 12, 9, 15 times as high as that on bare GCE, respectively. The large peak separation between ASA and ACE ( $0.31 \text{ V}$ ), and ACE and CAF ( $0.78 \text{ V}$ ) are acceptable for their simultaneous determination in the mixture. This is due to the increase in the surface area, macroporous structure, and functionality in  $\text{CoFe}_2\text{O}_4$  compared with bare GCE. Therefore, cobalt ferrite is expected to be a potential electrode modifier for the simultaneous determination of ASA, ACE, and CAF.

### 3.3 Effect of pH

The electrochemical signals were measured in the pH range of  $2.8$ – $6.4$  (Fig. 10a). The peak current of ASA decreases slightly first as pH increases from  $2.8$  to  $ac$ .  $4.6$  and then declines significantly as pH increased further to  $6.4$ . The varying peak current of ACE exhibits nearly the same trend as that of ASA except for a large decline between pH  $3.9$  and pH  $4.6$ . While at pH  $3.9$ , the peak current of CAF reaches a maximum at pH  $3.9$  and then declines like that of ASA and ACE (Fig. 10b). Therefore, pH  $3.9$  ( $\approx 4$ ) was selected for further experiments.

The increase in pH causes the oxidation peak potential to shift to less positive potential, inferring that protons are involved in the oxidation process (Fig. 10a). At  $298 \text{ K}$ , the Nernst equation expresses the relationship between  $E_p$  and pH as follows:



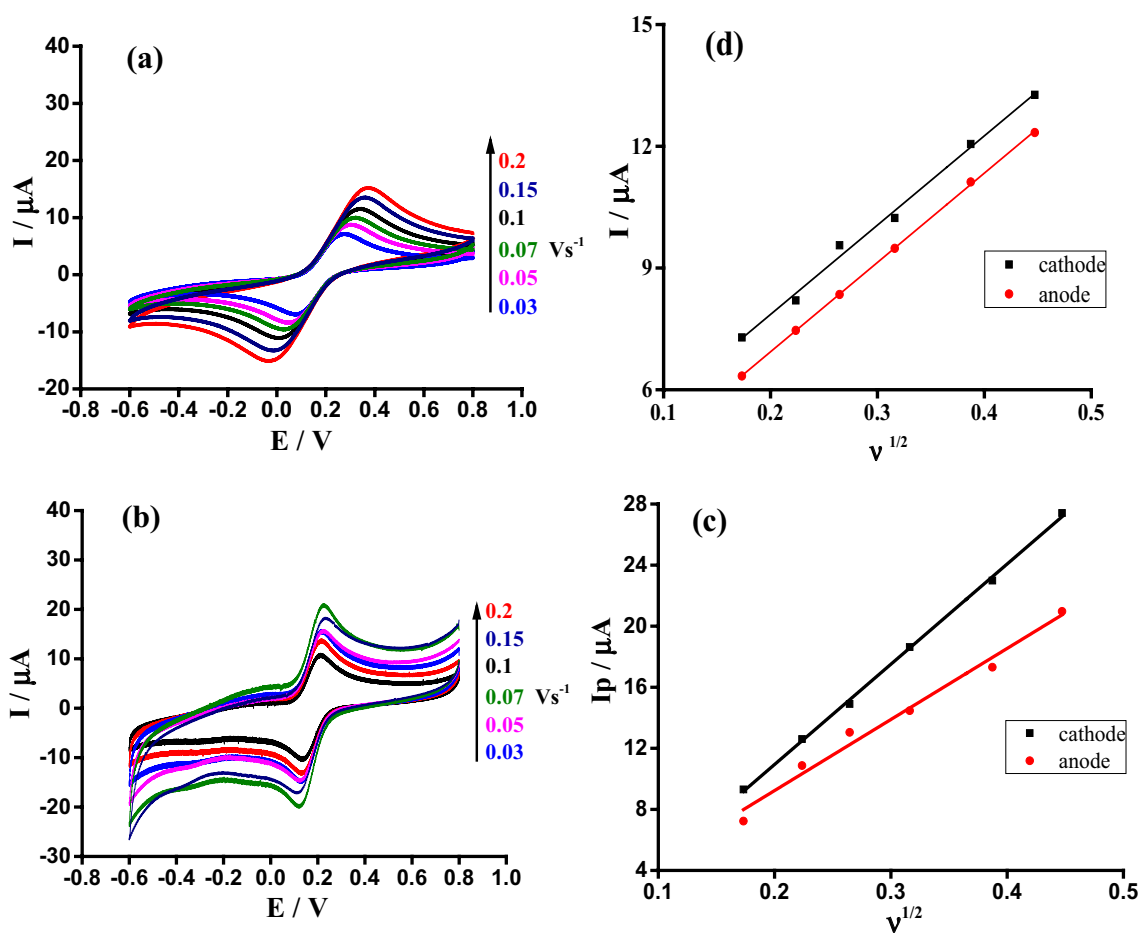


**Fig. 8** Cyclic voltammograms of **a** bare GCE; **b**  $\text{Co}_2\text{Fe}_2\text{O}_4/\text{GCE}$  at various scan rates; **c** the plot of peak current versus square root of scan rate at  $\text{Co}_2\text{Fe}_2\text{O}_4/\text{GCE}$ ; **d** the plot of peak current versus square root of scan rate at bare GCE (1 mM  $\text{K}_3[\text{Fe}(\text{CN})_6]/\text{K}_4[\text{Fe}(\text{CN})_6]$  in 0.1 M KCl)

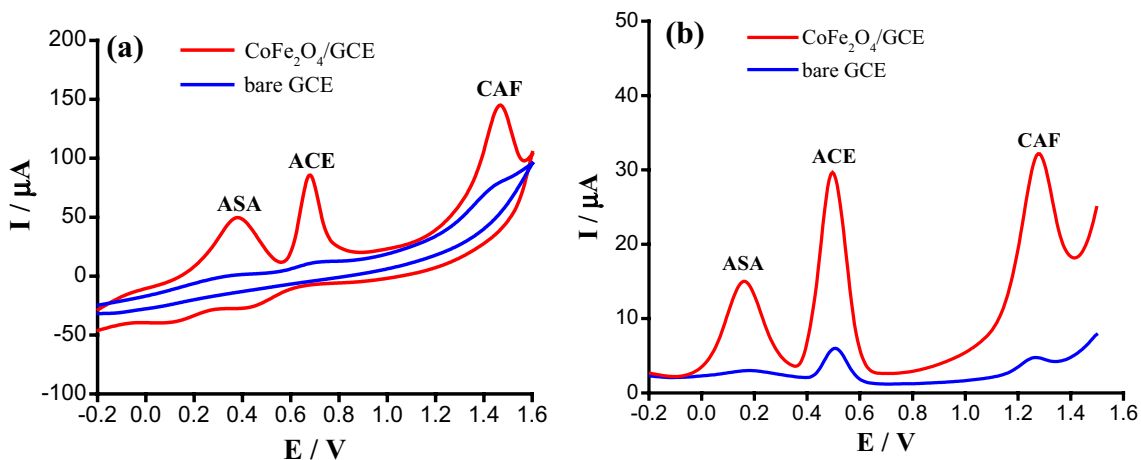


**Fig. 9** **a** Cyclic voltammograms (CVs) and **b** differential pulse voltammetry (DPV) at bare GCE and  $\text{Co}_2\text{Fe}_2\text{O}_4/\text{GCE}$  in 0.2 M B-R BS pH 4 containing an equal concentration of  $10^{-4}$  M ASA, ACE, and CAF



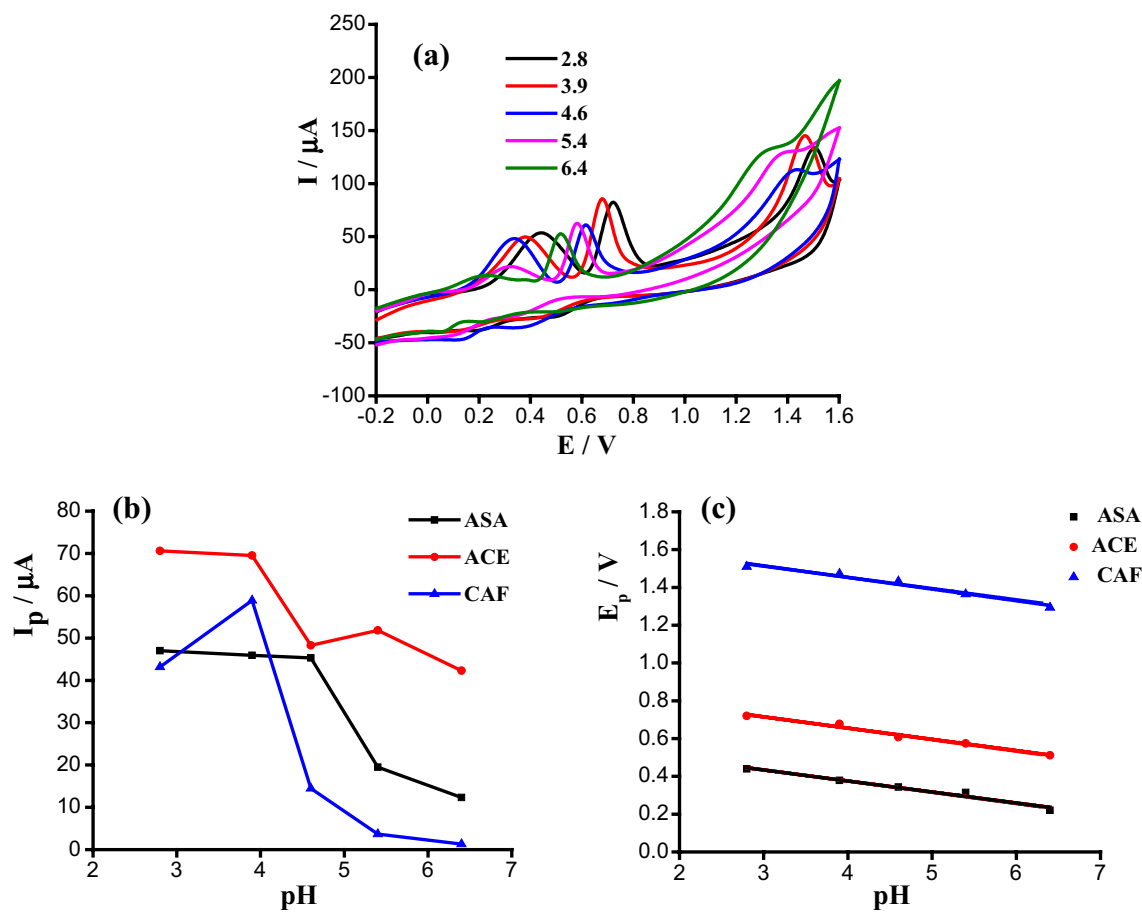


**Fig. 10** a Cyclic voltammograms of CoFe<sub>2</sub>O<sub>4</sub>/GCE in 0.2 M B-R BS pH 4 containing an equal concentration of 10<sup>-4</sup> M ASA, ACE, and CAF; b pH dependence on peak current ( $I_p$ ); c linear plot of  $E_p$  vs. pH

$$E_p = E^0 + \frac{0.0591}{n} \cdot \log \frac{\text{Ox}^a}{\text{Red}^b} - 0.059 \cdot \frac{p}{n} \cdot \text{pH} \quad (5)$$

where  $E^0$  is the standard electrode potential;  $p$  and  $n$  are the numbers of protons and electrons involved in the electrode reaction, respectively; Ox and Red are the conjugated redox pairs.

The linear regression equations between  $E_p$  versus pH for the analytes are as follows (Fig. 10c):

$$E_{p, \text{ASA}} = 0.61 - 0.058 \cdot \text{pH}; r = 0.986 \quad (6)$$

$$E_{p, \text{ACE}} = 0.89 - 0.059 \cdot \text{pH}; r = 0.991 \quad (7)$$

$$E_{p, \text{CAF}} = 1.70 - 0.062 \cdot \text{pH}; r = 0.985 \quad (8)$$

As can be seen from Eqs. (6–8), the slopes of these plots are equal or close to the theoretical value of 0.059, indicating that an equal number of photons and electrons takes part in the redox process of ASA, ACE, and CAF.

### 3.4 Effect of scan rate

The relationship between peak current and scan rate can provide helpful information about the electrochemical mechanism. Therefore, the effect of scan rate ( $\nu$ ) on the peak current and peak potential was studied by using the CV method (Fig. 11a). The linear regression equations of the relationship between  $I_p$  and  $\nu$  are as follows:

$$I_{p, \text{ASA}} = (6.770 \pm 16.294) + (167.100 \pm 49.128) \cdot \nu; \quad r = 0.987; p = 0.002 \quad (9)$$

$$I_{p, \text{ACE}} = (1.960 \pm 12.185) + (280.200 \pm 36.740) \cdot \nu; \quad r = 0.997; p \leq 0.001 \quad (10)$$

$$I_{p, \text{CAF}} = (15.060 \pm 33.740) + (117.100 \pm 101.730) \cdot \nu; \quad r = 0.954; p = 0.012 \quad (11)$$

The highly linear relationship of the plots between  $I_p$  and  $\nu$  ( $r = 0.954$ – $0.997$ ;  $p < 0.05$ ) indicates that oxidation at CoFe<sub>2</sub>O<sub>4</sub>/GCE is adsorption-controlled (see Fig. 11b) [46].

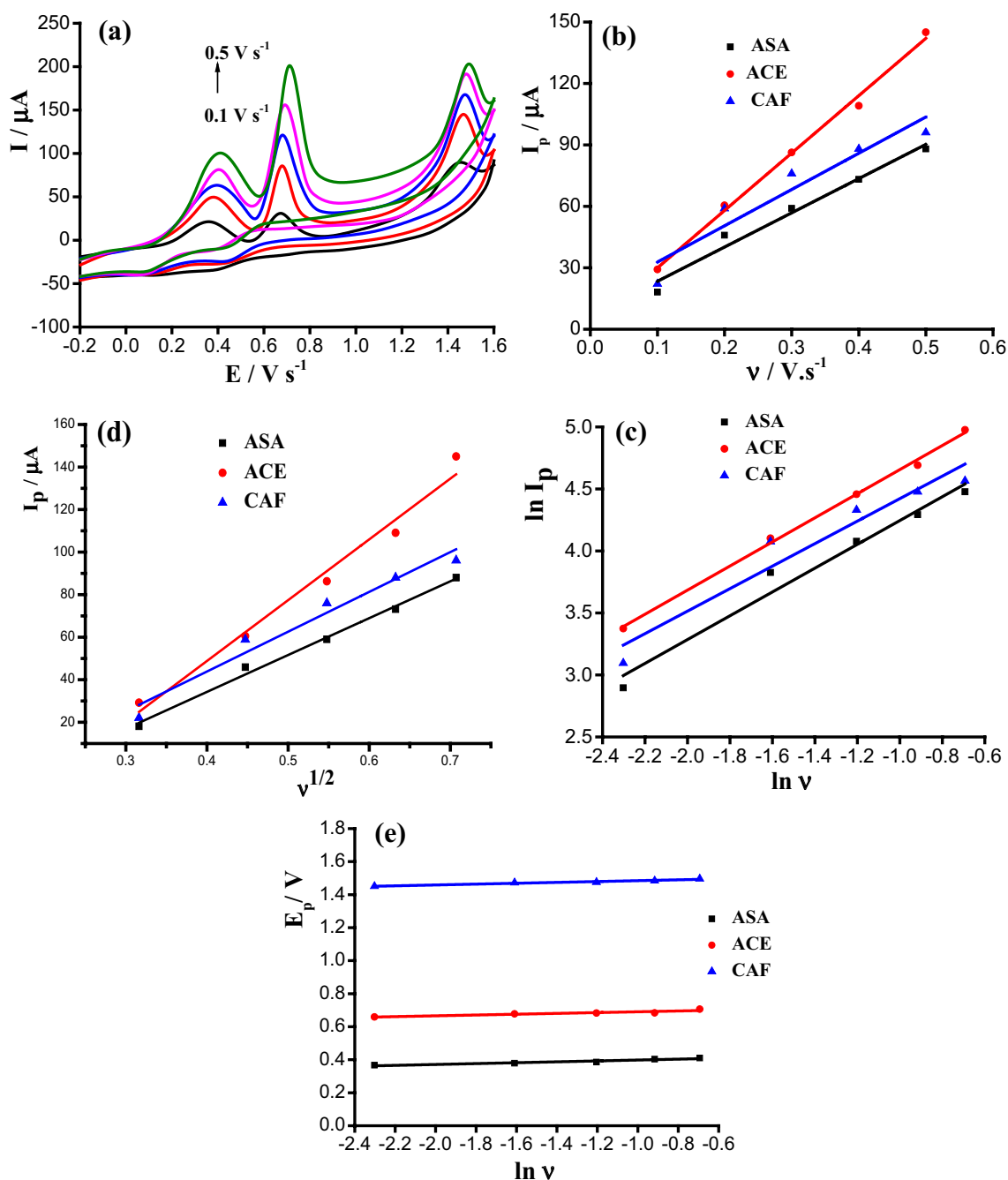


**Fig. 11** a Cyclic voltammograms of  $\text{CoFe}_2\text{O}_4/\text{GCE}$ ; b plot of  $I_p$  versus  $v$ ; c plot of  $\ln I_p$  versus  $\ln v$ ; d plot of  $I_p$  versus  $v^{1/2}$  e plot of  $E_p$  versus  $\ln v$  in 0.2 M B–R BS, pH 4 containing an equal concentration of  $10^{-4}$  M ASA, ACE, and CAF at various scan rates

The plots of  $\ln I_p$  versus  $\ln v$  or  $I_p$  versus  $v^{1/2}$  can provide information on whether a reaction is adsorption- or diffusion-controlled. Figure 11c shows the plots of the logarithm of the oxidation peaks of ASA, ACE, and CAF in 0.02 M B–R BS, pH 4 versus the logarithm of scan rate. The regression equations are as follows:

$$\ln I_{p,\text{ASA}} = 5.205 + 0.960 \cdot \ln v; r = 0.986; p = 0.002 \quad (12)$$

$$\ln I_{p,\text{ACE}} = 5.628 + 0.972 \cdot \ln v; r = 0.999; p \leq 0.001 \quad (13)$$

$$\ln I_{p,\text{CAF}} = 5.329 + 0.907 \cdot \ln v; r = 0.967; p = 0.007 \quad (14)$$

If the slope of the regression equations approaches 0.5, the reaction is supposed to be a diffusion-controlled electrode process, and if it approaches 1.0, the reaction is expected to be an adsorption-controlled process [47, 48]. In

our study, the slopes are very close to 1.0 (0.960 for ASA, 0.972 for ACE, and 0.907 for CAF), indicating that oxidation at  $\text{CoFe}_2\text{O}_4/\text{GCE}$  is an adsorption-controlled process. According to Soleymani et al., if the intercept of the plot of  $I_p$  versus  $v^{1/2}$  crosses the origin of the plot, the electrode process is controlled by diffusion; otherwise, it is adsorption-controlled [49]. In the scan rate range from 0.10 to  $0.50 \text{ V s}^{-1}$ ,  $I_p$  of ASA, ACE and CAF electrooxidation is linearly correlated with  $v^{1/2}$  following the equations (Fig. 11d):

$$I_{p,\text{ASA}} = (-35.054 \pm 13.665) + (173.338 \pm 24.950) \cdot v^{1/2}; r = 0.999; p \leq 0.001 \quad (15)$$

$$I_{p,\text{ACE}} = (-65.500 \pm 40.449) + (285.808 \pm 24.950) \cdot v^{1/2}; r = 0.990; p = 0.001 \quad (16)$$

$$I_{p,\text{CAF}} = (-31.020 \pm 30.335) + (187.194 \pm 66.338) \cdot v^{1/2}; r = 0.982; p = 0.003 \quad (17)$$

Equations (15–17) show that the relationship between the peak current and the square root of the scan rate is highly linear ( $r=0.982\text{--}0.999$ ;  $p<0.05$ ). The numbers in the parentheses are the 95% confident interval of the respective values. The intercepts of all the three equations are far less than zero, referring that the electrode oxidation is controlled by adsorption.

According to the analysis of the three relationships, namely  $I_p$  versus  $v$ ;  $\ln I_p$  versus  $\ln v$ ; and  $I_p$  versus  $v^{1/2}$ , we can conclude that the electrooxidation of ASA, ACE, and CAF on  $\text{CoFe}_2\text{O}_4/\text{GCE}$  is an adsorption-controlled process. This is characteristic for the electrode process, in which the electrochemical reaction precedes the homogenous chemical reaction [49].

According to the Laviron theory [50], for an irreversible anodic reaction, the relationship between  $E_p$  and  $v$  should be expressed as:

$$E_p = E^0 - \frac{R \cdot T}{(1-\alpha) \cdot n \cdot F} \cdot \ln \frac{R \cdot T \cdot K_s}{(1-\alpha) \cdot n \cdot F} + \frac{R \cdot T}{(1-\alpha) \cdot n \cdot F} \cdot \ln v \quad (18)$$

where  $E_0$  is the formal standard potential;  $\alpha$  is the charge transfer coefficient;  $n$  is the number of the electrons transferred;  $F$  is the Faraday constant ( $96,500 \text{ C mol}^{-1}$ );  $K_s$  is the standard heterogeneous reaction rate constant; and  $R$  and  $T$  are  $8.123 \text{ J mol K}^{-1}$ ,  $298 \text{ K}$ , respectively.

This relationship for the oxidation of ASA, ACE, and CAF in our study is as follows:

$$E_{p,\text{ASA}} = 0.425 + 0.027 \cdot \ln v; r = 0.962 \quad (19)$$

$$E_{p,\text{ACE}} = 0.715 + 0.024 \cdot \ln v; r = 0.920 \quad (20)$$

$$E_{p,\text{CAF}} = 1.511 + 0.027 \cdot \ln v; r = 0.977 \quad (21)$$

As can be seen from Eqs. (19–21), the plots of  $E_p$  versus  $\ln v$  are highly linearly related ( $r=0.920\text{--}0.960$ ,  $p<0.05$ ). The values of  $(1-n)\alpha$  can be calculated from the slopes of the plots (Fig. 11e), and they are 0.95, 1.05, and 0.95 for ASA, ACE, and CAF, respectively. For a totally irreversible process,  $\alpha$  is accepted to be 0.5. Therefore,  $n$  is approximately 1.9; 2.10, and 1.90 for ASA, ACE, and CAF, respectively. Since  $n$  is an integral, we accept that  $n$  equals 2. As a result, two protons and two electrons are involved in the redox process.

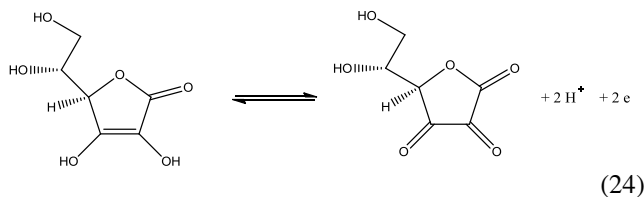
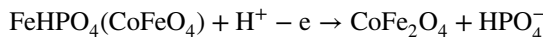
As mentioned above, the anodic peak current tends to decrease with increasing pH, and this indicates that the chemical reactions occur according to the electrochemical mechanism, in which the possible reaction between the buffer molecules and the oxidized form of the electrode is acceptable [49]. It is assumed that cobalt ferrite exhibits electrocatalytic activity as ferrite ( $\text{Fe}_3\text{O}_4$ ) [49, 51]. Then, the electrochemical behavior could involve the iron phosphate system. The  $\text{CoFe}_2\text{O}_4$  particles are directly oxidized at the electrode according to reaction (22).

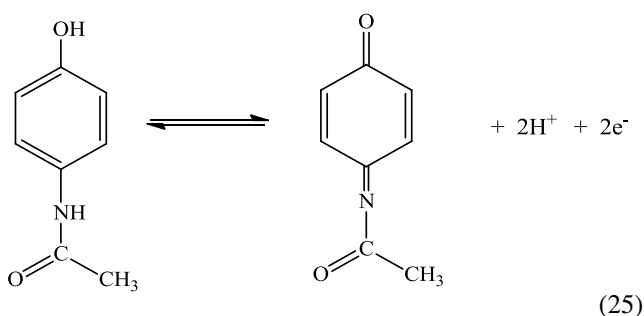


The as-produced  $\text{Fe}^{2+}$  ions react with the phosphate ions of the buffer.



The  $\text{FePO}_4$  solid at the electrode surface could be responsible for the electrocatalytic reaction

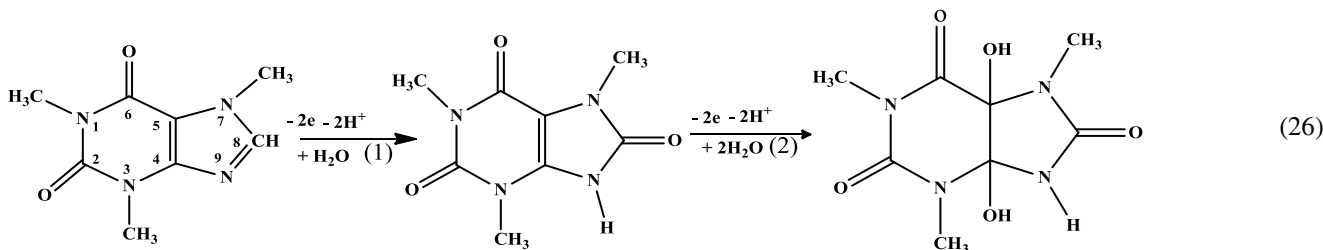




$\text{CoFe}_2\text{O}_4$  with a bigger number of redox-catalytic sites ( $\text{Fe}^{3+}/\text{Fe}^{2+}$ ), hierarchical structure, and large surface area enhances the adsorption effectively, and therefore, the oxidation of ASA, ACE, and CAF results in high electrochemical responses and a large peak separation. This process is illustrated in Fig. 12.

### 3.5 Interference study

The effect of several possible interfering compounds on the detection of ASA, ACE, and CAF was studied. DPV



CAF is oxidized in a two-step mechanism (reaction (26)). First,  $2\text{H}^+$ ,  $2\text{e}^-$  oxidation occurs at C-8 and N-9 atoms of caffeine and gives 8-oxy caffeine. Second, another  $2\text{e}^-$ ,  $2\text{H}^+$  oxidation gives 4,5-dihydroxy-8-oxy-caffeine [52]. Therefore, the oxidation of CAF with two electrons and two protons at  $\text{CoFe}_2\text{O}_4/\text{GCE}$  could be understood as the first step of this mechanism, and it also determines the rate of this reaction.

measurements were performed for the solution containing an equal concentration ( $10^{-6}$  M) of ASA, ACE, and CAF in 0.2 M B-R BS, pH 4 in the presence of an excess concentration of an interfering agent. The tolerance limit is assumed as the maximum concentration of the interferent brought about a relative standard error (RSD) less than 5%. In our study, 500 fold of  $\text{NaNO}_3$ ,  $\text{KNO}_3$ ,  $\text{CaCl}_2$ ,  $(\text{NH}_4)_2\text{SO}_4$  do not affect the selectivity, and no interfering effect is observed

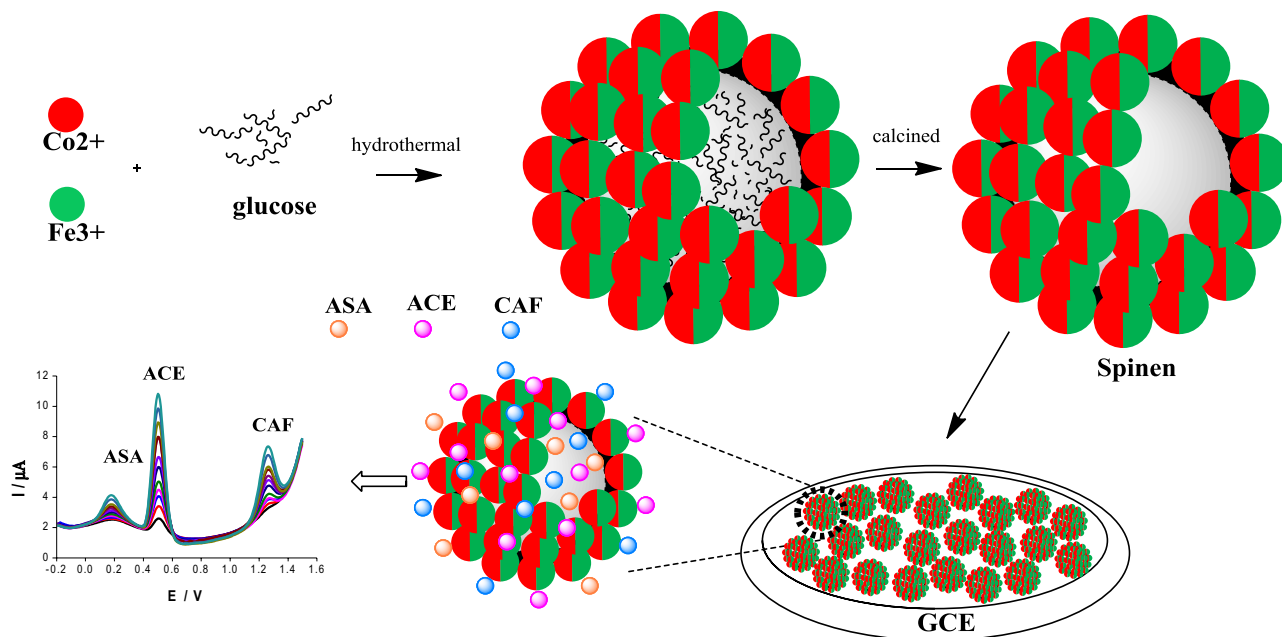
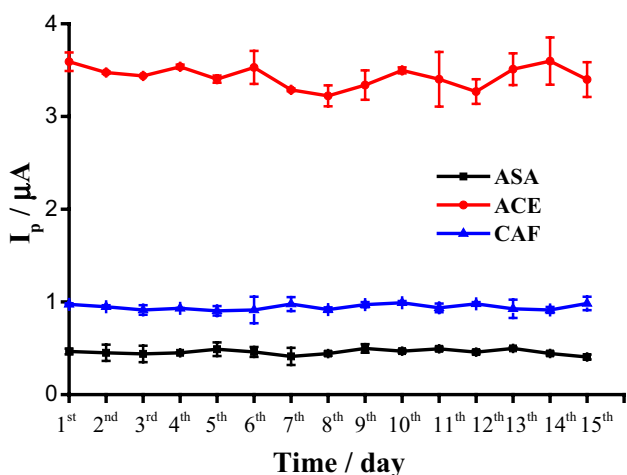


Fig. 12 Illustration of ASA, ACE, and CAF oxidation at  $\text{CoFe}_2\text{O}_4/\text{GCE}$

**Table 1** Effect of different interferences on peak currents ( $10^{-6}$  M ASA, ACE, and CAF in 0.2 B–R BS, pH 4)

Interferent	RSD (%)			Tolerance (mM)
	ASA	ACE	CAF	
Glucose	−4.9	−2.8	−1.9	152
Benzoic acid	1.2	0.2	4.3	180
Glutamic acid	3	−0.3	4.1	200
NaNO <sub>3</sub>	−3.6	−4.3	−1	500
KNO <sub>3</sub>	−1.6	3.8	0.6	500
KHCO <sub>3</sub>	1.1	4.1	−2.3	500
(NH <sub>4</sub> ) <sub>2</sub> SO <sub>4</sub>	0.3	−1.0	−2.7	500
CaCl <sub>2</sub>	−3.5	2.1	−0.8	500

**Fig. 13** Long-term stability of CoFe<sub>2</sub>O<sub>4</sub>/GCE during 15 consecutive days

at 152 fold of glucose, 180 fold of benzoic acid, and 200 fold of glutamic acid. RSD varies between −4.9 and 4.3% (Table 1). This reveals the acceptable selectivity of the CoFe<sub>2</sub>O<sub>4</sub> electrode even in the presence of high concentrations of other species.

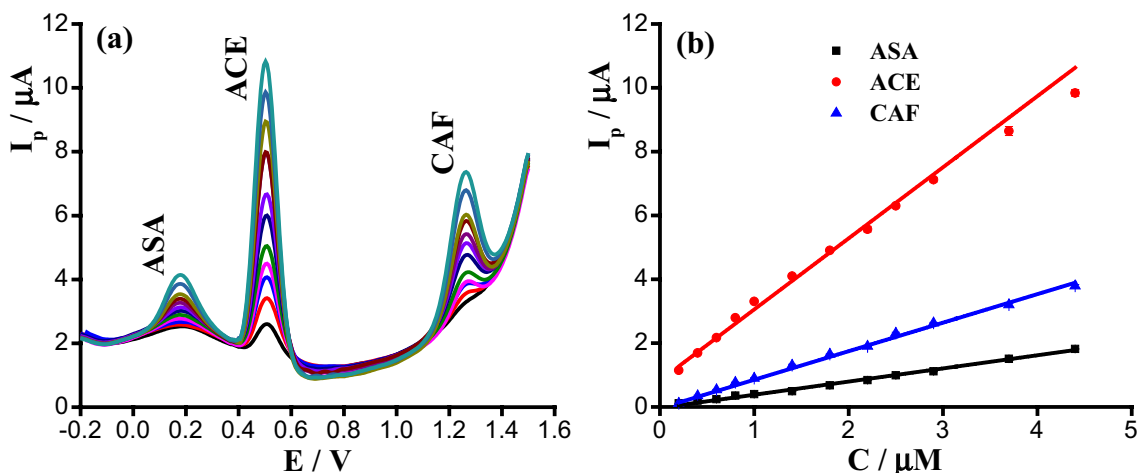
### 3.6 Long-term stability and limit of detection (LOD)

The peak current was recorded for ASA, ACE, and CAF oxidation at the modified GCE in the 0.2 M B–R BS containing the spiked solution of an equal concentration ( $10^{-4}$  M) of ASA, ACE, and CAF at different times to assess the long-term stability of CoFe<sub>2</sub>O<sub>4</sub>/GCE. Figure 13 presents the peak currents measured with time (day). The error bars are the standard deviation of sixteen experiments (of the peak current for ASA, ACE, and CAF was 6.7, 5.6, and 7.2%, respectively) using the same CoFe<sub>2</sub>O<sub>4</sub>/GCE for all the measurements. The relevant values of RSD infer that CoFe<sub>2</sub>O<sub>4</sub>/GCE has long-term stability and acceptable sensitivity for the analysis of real samples.

Since all peaks could be resolved at CoFe<sub>2</sub>O<sub>4</sub>/GCE, the simultaneous detection of the compounds was conducted. Figure 14a presents the DPV recorded for the simultaneous addition of ASA, ACE, and CAF in the increasing concentration in the range 0.2–4.4 μM. The plots of  $I_{p,ASA}$ ,  $I_{p,ACE}$ , and  $I_{p,CAF}$  versus ASA, ACE, and CAF concentration are shown in Fig. 14b. Their linear regression equations are as follows:

$$I_{p,ASA} = (-3.03 \pm 0.02) + (0.412 \pm 0.009) \cdot C_{ASA}; r = 0.998 \quad (27)$$

$$I_{p,ACE} = (0.83 \pm 0.06) + (2.23 \pm 0.05) \cdot C_{ACE}; r = 0.997 \quad (28)$$

**Fig. 14** **a** Differential pulse voltammetric responses at CoFe<sub>2</sub>O<sub>4</sub>/GCE in 0.2 B–R BS, pH 4 containing the equal concentration varying from 0.2 to 4.4 μM; **b** plot of anodic peak current as a function of analyte concentration

$$I_{p,CAE} = (-0.04 \pm 0.02) + (0.89 \pm 0.02) \cdot C_{CAF}; r = 0.998 \quad (29)$$

The LOD of ASA, ACE, and CAF [three times of the standard deviation of the blank over sensitivity ( $3 s m^{-1}$ )] is  $0.313 \mu M$ ,  $0.267 \mu M$ , and  $0.226 \mu M$ , respectively. The sensitivity of the ASA, ACE, and CAF determination is 0.41, 2.23 and 0.89, respectively.

Table 2 compares the linear range and LOD for our electrode with several modified electrodes reported previously. The data show that the linear range obtained in this work with  $CoFe_2O_4/GCE$  is much smaller, whereas LODs are compatible or lower than those of other works.

### 3.7 Determination of ASA, ACE, and CAF in pharmaceutical preparations and beverages

As for the real samples, those containing simultaneously ASA, ACE, and CAF are unavailable, but ACE and CAF, or ASA and ACE are found in several pharmaceutical formulas

(Table 3), and ASA and CAF are found in certain beverages. Therefore, six commercial pharmaceutical and three beverage samples were used to qualify the method (Table 4). The determination was carried out using the standard addition method. The analysis was performed three times under the same conditions. The recoveries of the analytes in the real samples were calculated to estimate the accuracy of the proposed method. Then, known amounts of both ACE and CAF, ASA and ACE, or ASA and CAF were added to the samples and the analytes were simultaneously analyzed again using the standard addition method with the proposed DPV method. The recovery is in the range of 95–106%. The analytes were also determined by using HPLC for comparison. The content of ASA, ACE, and CAF in the samples determined using the proposed method and the HPLC method is in a good agreement. The recovery is also acceptable. From these results, we can conclude that the  $CoFe_2O_4/GCE$  electrode is capable of the simultaneous analysis of pharmaceutical and beverage samples.

**Table 2** Performance comparison of the proposed DPV method for ARA, ACE, and CAF with other electrodes

Modified electrodes	Linear range ( $\mu M$ )			LOD ( $\mu M$ )			References
	ASA	ACE	CAF	ASA	ACE	CAF	
$CoFe_2O_4/graphene/GPE$	0.03–12	0.03–12	0.03–12	N/a	0.025	N/a	[52]
Flavonoid nanostructured modified/GCE	N/a	0.9–80	10–110	N/a	0.78	3.54	[53]
Poly(4-amino-3-hydroxynaphthalene sulfonic acid)/GCE	N/a	10–125	10–1250	N/a	0.45	0.79	[54]
Pd/aluminum electrode	0.1–3000	0.1–3000	N/a	5	5	N/a	[55]
ErGO/GCE	0.2–4.4	0.2–4.4	0.2–4	0.360	0.250	0.230	[32]
$MnFe_2O_4/nitrogen\ doped\ carbon\ nanotubes/GCE$	2–100	1–100	1–1100	1.800	0.830	0.830	[16]
$CuO/graphene/GCE$	0.025–5.5	0.025–5.5	0.025–5.5	0.011	0.008	0.01	[17]
$CoFe_2O_4/GCE$	0.2–4.4	0.2–4.4	0.2–4.4	0.313	0.267	0.226	The present study

N/a not applicable

**Table 3** Results of ASA, ACE and CAF determination in the pharmaceutical preparations using the proposed DPV and HPLC method

Notation	Analytes	Amount labeled ( $mg\ tablet^{-1}$ )	Methods		
			DPV <sup>a</sup>	Rev	HPLC <sup>a</sup>
Acetab extra	ACE	500	$492 \pm 5$	106	$490 \pm 1$
	CAF	65	$64.5 \pm 0.9$	96	$65.8 \pm 0.5$
Flucoldstad	ACE	500	$498 \pm 4$	98	$496.1 \pm 0.9$
	CAF	25	$24 \pm 1$	100	$23.6 \pm 0.1$
Pancelxim extra	ACE	500	$494 \pm 4$	104	$492 \pm 2$
	CAF	65	$64.2 \pm 0.3$	96	$63.7 \pm 0.2$
Hapacol Sac. 150 mg kids	ASA	75	$76 \pm 6$	98	$74 \pm 1$
	ACE	150	$150 \pm 4$	102	$151 \pm 2$
Doliprane vitamin C 500MG/150MG	ASA	150	$147.6 \pm 5$	98	$146.1 \pm 0.9$
	ACE	500	$495 \pm 6$	96	$494 \pm 3$
Effergan vitamin C	ASA	200	$197 \pm 4$	102	$195 \pm 2$
	ACE	330	$330 \pm 5$	98	$329 \pm 4$

<sup>a</sup>Average of three measurements  $\pm$  standard deviation

**Table 4** Results of ASA, ACE and CAF determination in the beverage samples using the proposed DPV and HPLC method

Notation	Analytes	Amount labeled (mg tablet <sup>-1</sup> )	Methods		
			DPV <sup>a</sup>	Rev	HPLC <sup>a</sup>
Number one	ASA	N/a	204.9 ± 3.3	106	206.8 ± 0.2
	CAF	≤ 758	22.5 ± 1.9	98	21.67 ± 0.02
Sting max gold	ACE	N/a	180.4 ± 3.8	92	179.5 ± 0.5
	CAF	300	29.6 ± 7.2	100	30.73 ± 0.05
Wake-up 247	ASA	N/a	259.3 ± 5.1	104	361 ± 8
	CAF	300	33.1 ± 6.4	94	32.49 ± 0.02

<sup>a</sup>Average of three measurements ± standard deviation

## 4 Conclusions

The synthesis of cobalt ferrite hollow spheres was performed using the carbonaceous microspheres prepared from the glucose solution as a sacrificial template. The Fe/Co ratio in cobalt ferrite could be controlled by varying the initial Fe/Co ratio. The resulting CoFe<sub>2</sub>O<sub>4</sub> possesses a hierarchical structure of hollow spheres, large specific areas, and high magnetic saturation. The CoFe<sub>2</sub>O<sub>4</sub> hollow spheres were used to develop a modified electrode, and it is promising for the ASA, ACE, and CAF detection with such advantages as high sensitivity and stability and low detection limit. The proposed DPV method can be easily performed with acceptable precision and accuracy when employed to pharmaceutical preparations and beverage samples.

**Acknowledgements** This research was sponsored by Hue University under Decision No. 1208/QĐ-DHH.

## References

- S.S. Gropper, J.L. Smith, *Advanced Nutrition and Human Metabolism* (Cengage Learning, Boston, 2012)
- A. Nehlig, J.-L. Daval, G. Debry, Caffeine and the central nervous system: mechanisms of action, biochemical, metabolic and psychostimulant effects. *Brain Res. Rev.* **17**, 139–170 (1992)
- P. Association, *Diagnostic and Statistical Manual of Mental Disorders* (Author, Washington, DC, 2000)
- V.K. Gupta, A.K. Jain, S.K. Shoor, Multiwall carbon nanotube modified glassy carbon electrode as voltammetric sensor for the simultaneous determination of ascorbic acid and caffeine. *Electrochim. Acta* **93**, 248–253 (2013)
- J. Wang, M. Li, Z. Shi, N. Li, Z. Gu, Direct electrochemistry of cytochrome c at a glassy carbon electrode modified with single-wall carbon nanotubes. *Anal. Chem.* **74**, 1993–1997 (2002)
- A. Afkhami, H. Khoshshafar, H. Bagheri, T. Madrakian, Facile simultaneous electrochemical determination of codeine and acetaminophen in pharmaceutical samples and biological fluids by graphene–CoFe<sub>2</sub>O<sub>4</sub> nanocomposite modified carbon paste electrode. *Sens. Actuators B* **203**, 909–918 (2014)
- M. Mazloum-Ardakani, M.A. Sheikh-Mohseni, M. Abdollahi-Alibeik, A. Benvidi, Application of nanosized MCM-41 to fabrication of a nanostructured electrochemical sensor for the simultaneous determination of levodopa and carbidopa. *Analyst* **137**, 1950–1955 (2012)
- I. Cesarino, G. Marino, J. do Rosário Matos, E.T.G. Cavalheiro, Evaluation of a carbon paste electrode modified with organofunctionalised SBA-15 nanostructured silica in the simultaneous determination of divalent lead, copper and mercury ions. *Talanta* **75**, 15–21 (2008)
- M.-J. Song, S.W. Hwang, D. Whang, Non-enzymatic electrochemical CuO nanoflowers sensor for hydrogen peroxide detection. *Talanta* **80**, 1648–1652 (2010)
- S. Thiagarajan, T.H. Tsai, S.-M. Chen, Electrochemical fabrication of nano manganese oxide modified electrode for the detection of H<sub>2</sub>O<sub>2</sub>. *Int. J. Electrochem. Sci.* **6**, 2235–2245 (2011)
- J. Zhou, X. Li, L. Yang, S. Yan, M. Wang, D. Cheng, Q. Chen, Y. Dong, P. Liu, W. Cai, The Cu-MOF-199/single-walled carbon nanotubes modified electrode for simultaneous determination of hydroquinone and catechol with extended linear ranges and lower detection limits. *Anal. Chim. Acta* **899**, 57–65 (2015)
- Y. Jin, C. Ge, X. Li, M. Zhang, G. Xu, D. Li, A sensitive electrochemical sensor based on ZIF-8–acetylene black–chitosan nanocomposites for rutin detection. *RSC Adv.* **8**, 32740–32746 (2018)
- R.N. Goyal, S.P. Singh, Voltammetric determination of paracetamol at C60-modified glassy carbon electrode. *Electrochim. Acta* **51**, 3008–3012 (2006)
- P.R. Dalmasso, M.L. Pedano, G.A. Rivas, Electrochemical determination of ascorbic acid and paracetamol in pharmaceutical formulations using a glassy carbon electrode modified with multi-wall carbon nanotubes dispersed in polyhistidine. *Sens. Actuators B* **173**, 732–736 (2012)
- O.-W. Lau, S.-F. Luk, Y.-M. Cheung, Simultaneous determination of ascorbic acid, caffeine and paracetamol in drug formulations by differential-pulse voltammetry using a glassy carbon electrode. *Analyst* **114**, 1047–1051 (1989)
- D.M. Fernandes, N. Silva, C. Pereira, C. Moura, J.M.C.S. Magalhães, B. Bachiller-Baeza, I. Rodríguez-Ramos, A. Guerrero-Ruiz, C. Delerue-Matos, C. Freire, MnFe<sub>2</sub>O<sub>4</sub>@CNT-N as novel electrochemical nanosensor for determination of caffeine, acetaminophen and ascorbic acid. *Sens. Actuators B* **218**, 128–136 (2015)
- Z.M. Khoshhesab, Simultaneous electrochemical determination of acetaminophen, caffeine and ascorbic acid using a new electrochemical sensor based on CuO–graphene nanocomposite. *RSC Adv.* **5**, 95140–95148 (2015)
- F. Liu, S. Laurent, A. Roch, L. Vander Elst, R.N. Muller, Size-controlled synthesis of CoFe<sub>2</sub>O<sub>4</sub> nanoparticles potential contrast agent for MRI and investigation on their size-dependent magnetic properties. *J. Nanomater.* **2013**, 127 (2013)
- H. Wei, D. Ding, X. Yan, J. Guo, L. Shao, H. Chen, L. Sun, H.A. Colorado, S. Wei, Z. Guo, Tungsten trioxide/zinc tungstate bilayers: electrochromic behaviors, energy storage and electron transfer. *Electrochim. Acta* **132**, 58–66 (2014)

20. P. Lavela, J.L. Tirado,  $\text{CoFe}_2\text{O}_4$  and  $\text{NiFe}_2\text{O}_4$  synthesized by sol-gel procedures for their use as anode materials for Li ion batteries. *J. Power Sources* **172**, 379–387 (2007)
21. M. Houshiar, F. Zebhi, Z.J. Razi, A. Alidoust, Z. Askari, Synthesis of cobalt ferrite ( $\text{CoFe}_2\text{O}_4$ ) nanoparticles using combustion, coprecipitation, and precipitation methods: a comparison study of size, structural, and magnetic properties. *J. Magn. Magn. Mater.* **371**, 43–48 (2014)
22. P. Laokul, S. Arthan, S. Maensiri, E. Swatsitang, Magnetic and optical properties of  $\text{CoFe}_2\text{O}_4$  nanoparticles synthesized by reverse micelle microemulsion method. *J. Supercond. Nov. Magn.* **28**, 2483–2489 (2015)
23. W. Baaziz, B.P. Pichon, Y. Liu, J.-M. Grenèche, C. Ulhaq-Bouillet, E. Terrier, N. Bergeard, V. Halté, C. Boeglin, F. Choueikani, Tuning of synthesis conditions by thermal decomposition toward core-shell  $\text{Co}_x\text{Fe}_{1-x}\text{O}@ \text{Co}_y\text{Fe}_{3-y}\text{O}_4$  and  $\text{CoFe}_2\text{O}_4$  nanoparticles with spherical and cubic shapes. *Chem. Mater.* **26**, 5063–5073 (2014)
24. I. Sharifi, H. Shokrollahi, M.M. Doroodmand, R. Safi, Magnetic and structural studies on  $\text{CoFe}_2\text{O}_4$  nanoparticles synthesized by co-precipitation, normal micelles and reverse micelles methods. *J. Magn. Magn. Mater.* **324**, 1854–1861 (2012)
25. H. Yang, X. Zhang, A. Tang, G. Qiu, Cobalt ferrite nanoparticles prepared by coprecipitation/mechanicochemical treatment. *Chem. Lett.* **33**, 826–827 (2004)
26. Z. Chen, L. Gao, Synthesis and magnetic properties of  $\text{CoFe}_2\text{O}_4$  nanoparticles by using PEG as surfactant additive. *Mater. Sci. Eng. B* **141**, 82–86 (2007)
27. M.M. El-Okr, M.A. Salem, M.S. Salim, R.M. El-Okr, M. Ashoush, H.M. Talaat, Synthesis of cobalt ferrite nano-particles and their magnetic characterization. *J. Magn. Magn. Mater.* **323**, 920–926 (2011)
28. D. Wang, C. Song, Z. Hu, X. Fu, Fabrication of hollow spheres and thin films of nickel hydroxide and nickel oxide with hierarchical structures. *J. Phys. Chem. B* **109**, 1125–1129 (2005)
29. X. Peng, Green chemical approaches toward high-quality semiconductor nanocrystals. *Chem. Eur. J.* **8**, 334–339 (2002)
30. X. Sun, Y. Li,  $\text{Ga}_2\text{O}_3$  and GaN semiconductor hollow spheres. *Angew. Chem.* **116**, 3915–3919 (2004)
31. X. Sun, J. Liu, Y. Li, Use of carbonaceous polysaccharide microspheres as templates for fabricating metal oxide hollow spheres. *Chem. Eur. J.* **12**, 2039–2047 (2006)
32. N.H. Phong, T.T.T. Toan, M.X. Tinh, T.N. Tuyen, T.X. Mau, D.Q. Khieu, Simultaneous voltammetric determination of ascorbic acid, paracetamol, and caffeine using electrochemically reduced graphene-oxide-modified electrode. *J. Nanomater.* **2018**, 1–15 (2018)
33. X. Sun, Y. Li, Colloidal carbon spheres and their core/shell structures with noble-metal nanoparticles. *Angew. Chem.* **116**, 607–611 (2004)
34. T. Dippong, E.A. Levei, O. Cadar, Preparation of  $\text{CoFe}_2\text{O}_4/\text{SiO}_2$  nanocomposites at low temperatures using short chain diols. *J. Chem.* **2017**, 1–11 (2017)
35. M.Y. Nassar, T.Y. Mohamed, I.S. Ahmed, N.M. Mohamed, M. Khatab, Hydrothermally synthesized  $\text{Co}_3\text{O}_4$ ,  $\alpha\text{-Fe}_2\text{O}_3$ , and  $\text{CoFe}_2\text{O}_4$  nanostructures: efficient nano-adsorbents for the removal of orange G textile dye from aqueous media. *J. Inorg. Organomet. Polym. Mater.* **27**, 1526–1537 (2017)
36. T. Sakaki, M. Shibata, T. Miki, H. Hirose, N. Hayashi, Reaction model of cellulose decomposition in near-critical water and fermentation of products. *Bioresour. Technol.* **58**, 197–202 (1996)
37. G.C.A. Luijkx, F. van Rantwijk, H. van Bekkum, M.J. Antal Jr., The role of deoxyhexonic acids in the hydrothermal decarboxylation of carbohydrates. *Carbohydr. Res.* **272**, 191–202 (1995)
38. D. Barreca, C. Massignan, S. Daolio, M. Fabrizio, C. Piccirillo, L. Armelao, E. Tondello, Composition and microstructure of cobalt oxide thin films obtained from a novel cobalt (II) precursor by chemical vapor deposition. *Chem. Mater.* **13**, 588–593 (2001)
39. T. Yamashita, P. Hayes, Analysis of XPS spectra of  $\text{Fe}^{2+}$  and  $\text{Fe}^{3+}$  ions in oxide materials. *Appl. Surf. Sci.* **254**, 2441–2449 (2008)
40. Y. Yang, H. Dong, Y. Wang, C. He, Y. Wang, X. Zhang, Synthesis of octahedral like Cu-BTC derivatives derived from MOF calcined under different atmosphere for application in CO oxidation. *J. Solid State Chem.* **258**, 582–587 (2018)
41. X. Zhang, H. Li, X. Lv, J. Xu, Y. Wang, C. He, N. Liu, Y. Yang, Y. Wang, Facile Synthesis of Highly Efficient Amorphous Mn-MIL-100 Catalysts: formation Mechanism and Structure Changes during Application in CO Oxidation. *Chem.: Eur. J.* **24**, 8822–8832 (2018)
42. K. Dukenbayev, I.V. Korolkov, D.I. Tishkevich, A.L. Kozlovskiy, S.V. Trukhanov, Y.G. Gorin, E.E. Shumskaya, E.Y. Kaniukov, D.A. Vinnik, M.V. Zdorovets,  $\text{Fe}_3\text{O}_4$  nanoparticles for complex targeted delivery and boron neutron capture therapy. *Nanomaterials* **9**, 494 (2019)
43. D.Z. Tulebayeva, A.L. Kozlovskiy, I.V. Korolkov, Y.G. Gorin, A.V. Kazantsev, L. Abylgazina, E.E. Shumskaya, E.Y. Kaniukov, M.V. Zdorovets, Modification of  $\text{Fe}_3\text{O}_4$  nanoparticles with carboranes. *Mater. Res. Express* **5**, 105011 (2018)
44. Y.P. Chang, C.L. Ren, J.C. Qu, X.G. Chen, Preparation and characterization of  $\text{Fe}_3\text{O}_4$ /graphene nanocomposite and investigation of its adsorption performance for aniline and p-chloroaniline. *Appl. Surf. Sci.* **261**, 504–509 (2012)
45. N.A. Kalanda, G.G. Gorokh, M.V. Yarmolich, A.A. Lozovenko, E.Y. Kanyukov, Magnetic and magnetoresistive properties of  $\text{Al}_2\text{O}_3\text{-Sr}_2\text{FeMoO}_6\text{-}\delta\text{-Al}_2\text{O}_3$  nanoheterostructures. *Phys. Solid State* **58**, 351–359 (2016)
46. S. Yang, L. Qu, R. Yang, J. Li, L. Yu, Modified glassy carbon electrode with Nafion/MWNTs as a sensitive voltammetric sensor for the determination of paeonol in pharmaceutical and biological samples. *J. Appl. Electrochem.* **40**, 1371–1378 (2010)
47. J. Xu, F. Shang, J.H.T. Luong, K.M. Razeeb, J.D. Glennon, Direct electrochemistry of horseradish peroxidase immobilized on a monolayer modified nanowire array electrode. *Biosens. Bioelectron.* **25**, 1313–1318 (2010)
48. A.J. Bard, L.R. Faulkner, J. Leddy, C.G. Zoski, *Electrochemical Methods: Fundamentals and Applications* (Wiley, New York, 1980)
49. J. Soleymani, M. Hasanzadeh, N. Shadjou, M.K. Jafari, J.V. Ghar-amaleki, M. Yadollahi, A. Jouyban, A new kinetic-mechanistic approach to elucidate electrooxidation of doxorubicin hydrochloride in unprocessed human fluids using magnetic graphene based nanocomposite modified glassy carbon electrode. *Mater. Sci. Eng. C* **61**, 638–650 (2016)
50. E. Laviron, General expression of the linear potential sweep voltammogram in the case of diffusionless electrochemical systems. *Electroanalysis* **101**, 19–28 (1979)
51. M. Hasanzadeh, N. Shadjou,  $(\text{Fe}_3\text{O}_4)\text{-graphene oxide-SO}_3\text{H}$  as a new magnetic nanocatalyst for electro-oxidation and determination of selected parabens. *J. Nanosci. Nanotechnol.* **13**, 4909–4916 (2013)
52. L. Švorc, P. Tomčík, J. Svítková, M. Rievaj, D. Bustin, Voltammetric determination of caffeine in beverage samples on bare boron-doped diamond electrode. *Food Chem.* **135**, 1198–1204 (2012)
53. M. Amiri-Aref, J.B. Raouf, R. Ojani, A highly sensitive electrochemical sensor for simultaneous voltammetric determination of noradrenaline, acetaminophen, xanthine and caffeine based on a flavonoid nanostructured modified glassy carbon electrode. *Sens. Actuators B* **192**, 634–641 (2014)



54. M. Tefera, A. Geto, M. Tessema, S. Admassie, Simultaneous determination of caffeine and paracetamol by square wave voltammetry at poly(4-amino-3-hydroxynaphthalene sulfonic acid)-modified glassy carbon electrode. *Food Chem.* **210**, 156–162 (2016)
55. M.H. Pournaghi-Azar, A. Saadatirad, Simultaneous determination of paracetamol, ascorbic acid and codeine by differential pulse

voltammetry on the aluminum electrode modified by thin layer of palladium. *Electroanalysis* **22**, 1592–1598 (2010)

**Publisher's Note** Springer Nature remains neutral with regard to jurisdictional claims in published maps and institutional affiliations.